Next Materials 13 (2026) 102657

Contents lists available at ScienceDirect

Next Materials

journal homepage: www.sciencedirect.com/journal/next-materials

Research article

Exploring *Artabotrys hexapetalus* seed particles as reinforcement for sustainable composites: Mechanical, thermal, water absorption and morphological studies

G. Rajeshkumar *, S. Prithika, S. Keerthika, T. Rohith Sai, S.V. Naren Prasaadh

Department of Mechanical Engineering, PSG Institute of Technology and Applied Research, Coimbatore, Tamil Nadu, India

ARTICLE INFO

Keywords:
Artabotrys hexapetalus
Seed particles
Natural fillers
Epoxy composites
Mechanical properties

ABSTRACT

The increasing awareness on the harmful effects of synthetic materials, the use of natural and renewable resources such as natural fillers as reinforcement in polymer composites has drawn significant attention in recent years. The current study involves the use one such natural filler obtained from *Artabotrys hexapetalus* seeds (AHS) for fabricating epoxy-based composites. The scanning electron microscopy (SEM), X-ray Diffraction (XRD) and Fourier Transform Infrared Spectroscopy (FTIR) analysis were performed to examine the microstructure, crystalline and chemical structure and intermolecular interaction of the seed particle. The crystalline size and crystalline index were found to be 14.03 nm and 10.8%, respectively. The outcomes of the composite's characterization showed that the mechanical properties including tensile, flexural, shore D hardness and impact strengths attained their peak values of 27.67 MPa, 44.39 MPa, 75 and 3.37 kJ/m^2, respectively when 10 wt% of particles were reinforced to epoxy. In addition, the thermal analysis indicated that the composites are majorly degraded at temperature range of 390 °C. The water absorption results indicate that the composite exhibits hydrophilic behavior and conforms to Fick's law of diffusion. The findings clearly demonstrate that the reinforcement of 10 wt% of AHS particles improves the overall properties of the composites and could be employed for light weight structural applications including automobile interiors, aircraft cabin interior panels, door frames and window panels.

1. Introduction

The rising demand for renewable, high-performance materials is driving research and industry towards eco-friendly substitutes to traditional synthetic reinforcements for making polymer-based composites [1]. This shift is mainly due to the negative environmental impact of synthetic reinforcements, including non-biodegradability, resource depletion and carbon dioxide emission of 8–9 kg CO_2 eq/kg during the production stage [2,3]. In this context, India, being one of the largest producers of agricultural waste, faces a significant challenge in managing the waste effectively, which leads to the burning of a large quantity of agro-waste and dumping, causing pollution to the environment [4,5]. Therefore, this study addresses the demand for renewable sources by valorizing the agro-waste as fillers (reinforcements) to produce bio-based composites. The necessity of adding reinforcement materials to neat polymers, due to their inability to withstand higher loads and stress transfer within the material [6]. Furthermore, the use of agricultural waste to produce bio-based composites establishes a valuable link between agriculture and industry [7], aligning with the UN Sustainable Development Goals (SDGs), particularly SDG−9 (Industry, Innovation and Infrastructure), and SDG−12 (Responsible Consumption and Production) [8,9]. Beyond the environmental advantages of these natural fillers, it also offers benefits such as abundance, lower production energy, cost and density [10,11].

In accordance with natural fiber reinforcements, natural particles or fillers are recently using as a potential reinforcement for polymer composites due to its advantages such as high surface area to volume ratio, higher strength to weight ratio, reducing void formation, increasing stiffness, better elevating dispersion with lesser weight percentage and restricting crack development in the matrix [12,13]. Vengatesh et al. [14] highlighted that the integration of *Terminalia arjuna* seed particles into vinyl ester significantly improved the composite's tensile and flexural strength with 15 wt% as optimum particle addition, emphasize that the inclusion of natural particles elevated the strength

* Corresponding author.
E-mail address: rajesh@psgitech.ac.in (G. Rajeshkumar).

https://doi.org/10.1016/j.nxmate.2026.102657
Received 25 April 2026; Received in revised form 19 June 2026; Accepted 27 June 2026
Available online 2 July 2026

and modulus of composites and suggesting that the optimum particle added composite can be used for structural, automobile, marine, and construction applications. Supporting this observation, Murugananthan et al. [15] documented the effect of *Caesalpinia bonducella* seed shell particles in epoxy matrix, revealing that the incorporation of seed particles yields more than 1.3 times the mechanical strength of pure epoxy. Furthermore, Rajeshkumar et al. [16] assessed the mechanical and thermal characteristics of *Phoenix sp.* particles incorporated epoxy composites. The result demonstrates that the 15 wt% particles added epoxy composites have higher thermal stability due to the development of char protective layer and composites loaded with 10 wt% particles showed 41.14% improvement in mechanical (tensile) strength.

During the development of composites, the matrix used plays an important role, which influences the technical performance and molding technology of the composite [17]. Epoxy resins are the predominantly used thermosetting material as a matrix due to their significance, such as strong bonding with the filler, adhesion strength, solvent resistance, high modulus, chemical resistance, elevated mechanical strength, and their unique chemical structure, causing them to form ring-opening polymerization that enhances the bond strength with the reinforcement [18,19].

Artabotrys hexapetalus, commonly known as climbing ylang-ylang belongs to the Annonacea family. It is an average-sized climbing shrub, largely cultivated in India and predominantly found in the southern part of China [20]. The flowers of this plant are used for their fragrance and its roots and fruits are valued for the production of a medical drug to treat malaria and scrofula [21]. During the extraction of the fruit, only the peel is utilized, while the seeds are discarded as waste. The seeds, which are oval to oblong and measure approximately 5 – 30 mm in length, contain lignin fiber cells that possess a resistance to thermal degradation, while the presence of stone cells contributes to hard seed coating, which enhances the overall structural strength of the seed [22]. Based on the above information, the *Artabotrys hexapetalus* seeds (AHS) can possess valuable structural characteristics suitable for reinforcement application in polymer composites, and it represents a promising biomass resource that can be utilized into value-added material under the waste-to-wealth concepts. In addition, natural seed-based fillers, including walnut shell, date seed, and tamarind seed particles, have been examined as reinforcements in polymer composites, research on *Artabotrys hexapetalus* seed particles is limited. To the authors' knowledge, no exhaustive investigation has documented the influence of AHS particles on the mechanical, thermal, and water absorption characteristics of epoxy composites.

Therefore, this study systematically examines the properties of AHS particles utilizing advanced characterization methods, such as X-ray Diffraction (XRD), Fourier Transform Infrared Spectroscopy (FTIR), Scanning Electron Microscopy (SEM), and Energy Dispersive X-ray Analysis (EDX). Additionally, the impact of different AHS particle loadings (5, 10, 15, and 20 wt%) on the performance of the composite is extensively evaluated. This includes static mechanical properties like tensile, flexural, impact, and hardness, as well as thermal behavior characterized by Thermogravimetric Analysis (TGA) and Differential Scanning Calorimetry (DSC). It also includes physical properties like water absorption, diffusion kinetics, and surface wettability (contact angle). The outcomes of this research are expected to find the ideal AHS loading that improves the composite's overall performance while maintaining the thermal stability and moisture uptake at acceptable levels, thereby demonstrating the potential of AHS particles reinforced composites as sustainable materials for lightweight structural applications.

2. Materials and methods

2.1. Materials

The fruit of *Artabotrys hexapetalus* were collected in the nearby areas of Coimbatore, Tamil Nadu, India. The seeds were manually separated from the fruit and sun-dried. Then the dried seeds were processed mechanically to obtain a powder form and it was used as a primary reinforcement material. The matrix consists of Epoxy polymer (LY556) and hardener (HY951), which were bought from Covai Seenu & Co., Coimbatore, Tamil Nadu, India. The properties of the LY556 resin in given in Table 1.

2.2. Methods

2.2.1. Fabrication of composites

The varied weight content (5, 10, 15, and 20 wt%) of AHS particle reinforced epoxy composites were fabricated using compression molding process. Epoxy resin, filler, and hardener are carefully mixed using a mechanical stirrer for 10 – 15 min at a stable speed of 400 rpm. The obtained mixture is evenly filled into the mold and is compressed under 5 bar pressure, then it was allowed to cure for 12 h to attain uniform thickness all over the plate. The composite plate was post-cured at room temperature for 14 days. Then, the samples were cut using the CNC machine according to ASTM standards for various property analysis. The fabrication process is illustrated in the Fig. 1.

2.2.2. Morphological analysis

For analyzing the morphological characteristics of particles and fractured samples, they were gold-coated to enhance conductivity and were tested using FE-SEM (CARL ZEISS (USA), having a resolution of 1.5 nm, accelerating voltage of 12 kV and working depth of 9–11.9 mm. In addition, energy dispersive X-ray spectroscopy (EDX) analysis was done along with the SEM to determine the elements present in the AHS particle. The EDX measures the intensity of X-ray emitted at a particular energy level. The obtained data is plotted in a graph for elemental analysis.

2.2.3. FTIR

FTIR spectroscopy determines the presence of functional groups, chemical and structural characteristic of the sample by subjecting it to an infrared radiation. At room temperature, the particle samples were analyzed using ATR SHIMADZU with a spectral output between 400 and 4000 cm^{-1}. The resolution of FTIR-Spectra was 4 cm^{-1}.

2.2.4. XRD

XRD method is used to investigate the crystalline structure of the material. In this experiment a scanning step time of 48 s and a continuous scanning mode with range 5° to 90° at 2θ angle were used. The analysis was done using 'powder X-ray diffraction' method, at 25 °C with 45 kV voltage and 30 mA current by employing copper (Cu) anode.

2.2.5. Mechanical testings

The tensile strength of the composites was examined using the universal testing machine (INSTRON 8801) with a capacity of 100 kN. The composite specimen was made in the size of 167 × 12 x 3 mm^3 with respect to the ASTM D638 standard. For flexural testing (using the same machine), the specimen was cut to the size of 125 × 12.7 × 3 mm^3 according to the ASTM D790 standards. For both the tests, the crosshead speed of 2.5 mm/min was maintained. The impact strength of samples (size of 64 ×12.7 ×3 mm^3) was determined by ASTM D256 standard using Izod impact testing equipment (International Equipments, India)

Table 1
Properties of LY556.

Property	Evaluation Method	Value	Unit
Appearance	Visual	Pale – yellow clear liquid.	-
Viscosity at 25 °C	IS 6749:1994	10,000 – 12,000	cP
Density at 25 °C	IS 6746:1994	1.15 – 1.20	gm/cm^3
Flash point	-	195	°C

Table 2
Degradation temperature of NE and AHS particle-based composites.

AHS particle content (wt%)	Degradation temperature (℃)
0	373
5	385
10	387.18
15	387.45
20	375

which consist of a pendulum of potential energy 2.71 J. These tests were performed for five specimens and the average value was recorded. A digital Shore D durometer with a measuring range of 0 – 100 HD, resolution of 0.5 HD, indenter depth of 0–1.5 mm, and test pressure of 0 – 45.5 N was used to identify the hardness of the samples. The firmly fixed sample on the slab was pressed vertically by an indenter needle and it was repeated five times at different spots and the mean value was reported.

2.2.6. TGA

TGA is a method to find the thermal stability of the sample. The sample was heated till it reaches 800 °C from the ambient conditions with a heating rate of 20 °C/min. The TGA curve was obtained representing the change in mass over a period of time as the temperature changes. The composite sample was kept under the nitrogen atmosphere and its thermal stability was determined by PerkinElmer – TGA 4000 analyzer.

2.2.7. DSC

DSC is a technique used to assess the thermal behavior of the sample. PerkinElmer, DSC 6000 was used in analyzing the thermal behavior with a heating rate of 10 °C/min operating from room temperature to 400 °C. The sample was kept under the N_2 atmosphere in an alumina crucible and analyzed to obtain DSC curves.

2.2.8. Water absorption

The samples which were made as per ASTM D570 standard of size 64 × 12.7 × 3 mm^3 was immersed in distilled water at room temperature to obtain its water absorbing capacity. The weight was measured at regular intervals and the percentage of moisture absorbed was calculated by observing the initial and final weights (Eq. 1).

$$\text{Water absorption}(\%) = \frac{(W_1 - W_0)}{W_0} \times 100 \quad (1)$$

where: W_1 – wet weight, in grams
W_0 – dry weight, in grams

2.3. Water contact angle

Kyowa Goniometer was used to find the water contact angle which signifies the wettability of the sample's surface. The measurement was carried out by placing a drop of deionized water on the sample surface and captured the same using a camera. Further the angle was obtained by image analysis software.

3. Results and discussion

3.1. Morphological analysis

The SEM images of the AHS particles is illustrated in Fig. 2(a). It signifies the presence of rough surface of the particles which is due to the agglomerates formed by the micro particles that exhibit amorphous nature. The increased surface roughness leads to efficient interlocking mechanisms between matrix and the reinforcement influencing the mechanical properties of the composites Small particles provide greater contact area with the matrix, initiating better interfacial attractions between the composite elements with establishing uniform dispersion of fillers that enhances the composite's mechanical stability [23,24]. The surface is observed to be irregular, fragmented and has sharp edges confirming that the material has undergone mechanical processing. The scattered pores ensure the efficient filling of resins exhibiting enhanced adhesion and stress transfer. In addition, the distribution of the particle size is depicted in the Fig. 2(b), which shows that the AHS particles used in this study has a mean size as 80 μm.

EDX analysis shown in Fig. 2(c) revealed the elemental composition of AHS particles. The existence of carbon (C), oxygen (O) and potassium (K) is found to be 55.69%, 39.65% and 2.48%, respectively by weight. Carbon being in major composition confirms the organic nature of the particle, influences the stiffness of the composites and provides better load bearing capacity [25]. The notable oxygen percent confirms the particle's hydrophilic nature and relates with the presence carbonyl and hydroxyl functional groups of particles correlates with the FTIR analysis.

3.2. XRD

The Fig. 3 illustrates the X-ray diffractogram, exhibiting the crystalline arrangement of AHS particles. The graph exhibited two distinct

Fig. 1. Fabrication methodology.

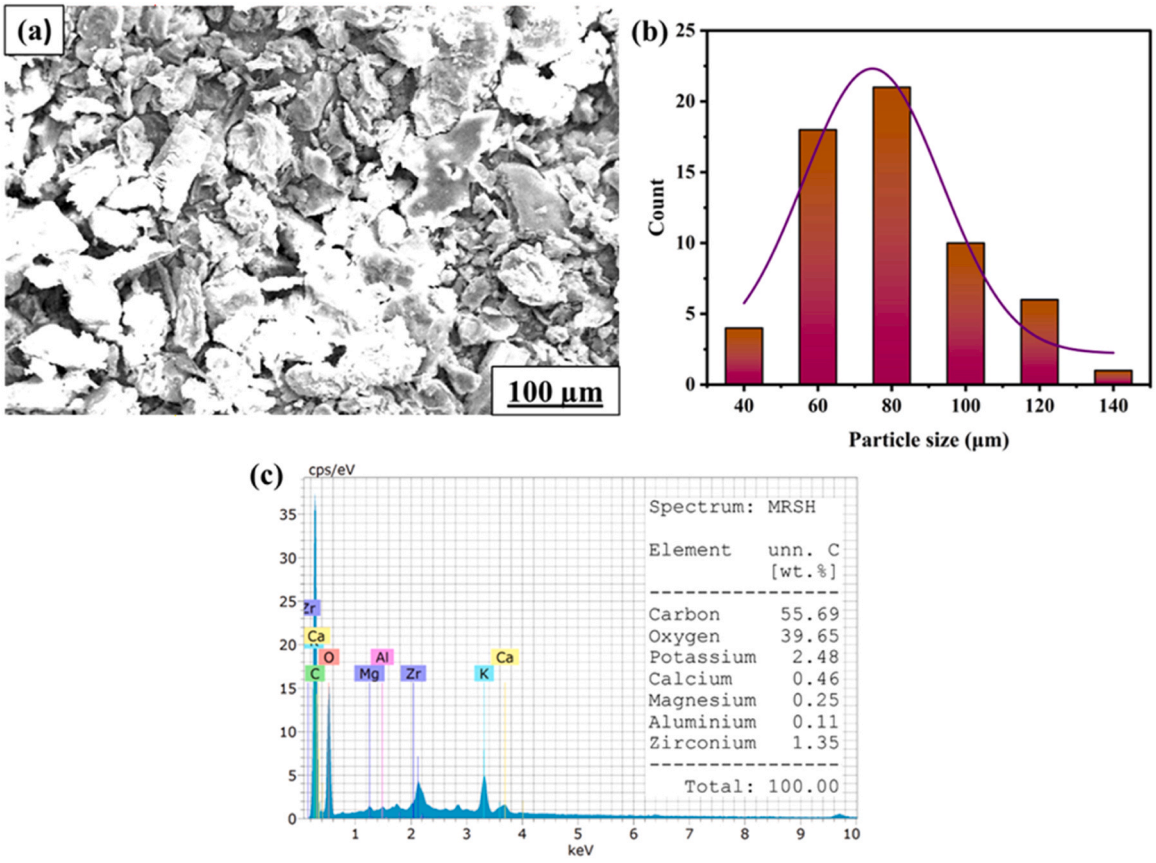

Fig. 2. Particle examination: (a) SEM, (b) Distribution of particle sizes, (c) EDX.

peaks at 2θ = 34.49° and 2θ = 22.29°, attributes to the (0 0 4) and (0 0 2) miller indices respectively, indicating the existence of cellulose I [26,27]. The crystallite size calculated using the Scherrer equation (Eq. 2) for the above two diffraction peaks are 14.03 nm and 21.97 nm, respectively.

$$D = \frac{k\lambda}{\beta \cos\theta} \tag{2}$$

where, D is the crystallite size, k represents shape factor, λ is the wavelength of X - ray, β is full width of half maximum in radians and θ is denotes the Bragg's angle or the incident angle of the X-ray. Furthermore, the crystalline index (CI) of AHS particles is determined (Eq. 3) to be 10.8% using deconvolution technique [28]. Lower crystalline size corresponds to a larger surface area and enhanced water exposure [29].

$$\mathrm{CI} = \frac{\sum \text{area under cystalline peak}}{\text{Total area}} \times 100 \tag{3}$$

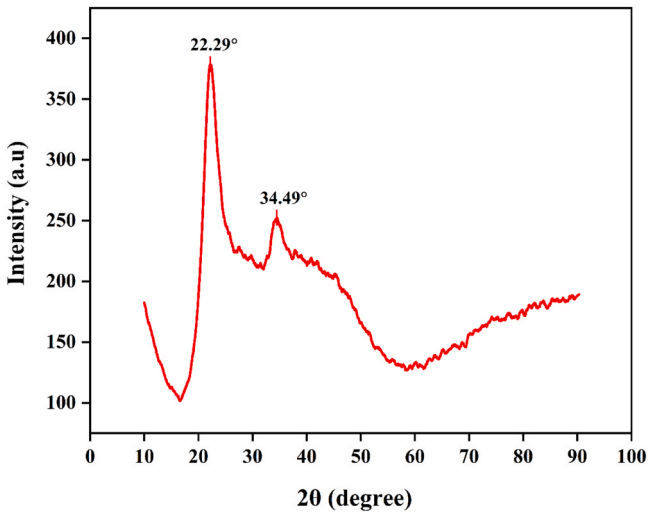

Fig. 3. XRD graph of AHS particles.

3.3. FTIR

Fig. 4 shows distinct peaks, each of which corresponds to different functional groups, bonding interaction, and molecular structure of AHS particles. The AHS particle contains hydroxyl groups in polysaccharides which is represented by a peak in the range of 3300–3350 cm^{-1}, caused by their stretching vibrations [30]. A peak at 2922 cm^{-1} is due to the existence of -OH and -CH stretching of α cellulose [31]. The peak at 1240 cm^{-1} and 3340 cm^{-1} is observed owning to asymmetrical stretching vibration of C-O-C and -OH stretching vibrations, respectively. At 1733 cm^{-1} the peak corresponds to C═O stretching vibrations of carboxylic acid and amide [32]. The peak at 1030 cm^{-1} is correlated with C-O-C and C-O stretching vibrations, which indicate the existence of ether linkages and polysaccharide backbones [33]. The presence of aromatic ring in lignin is the reason for the peak at 1552 cm^{-1} [6]. These functional groups have a significant influence on thermal stability, hydrophilicity and interfacial adhesion in composite application.

3.4. Mechanical properties

The Tensile Strength (TS) and Tensile Modulus (TM) of the composites loaded with AHS particles in different proportions is illustrated in Fig. 5(a). The TS and TM of neat epoxy (NE) is found to be 19.15 MPa and 1.85 GPa, respectively, when it was reinforced with 5 wt% AHS

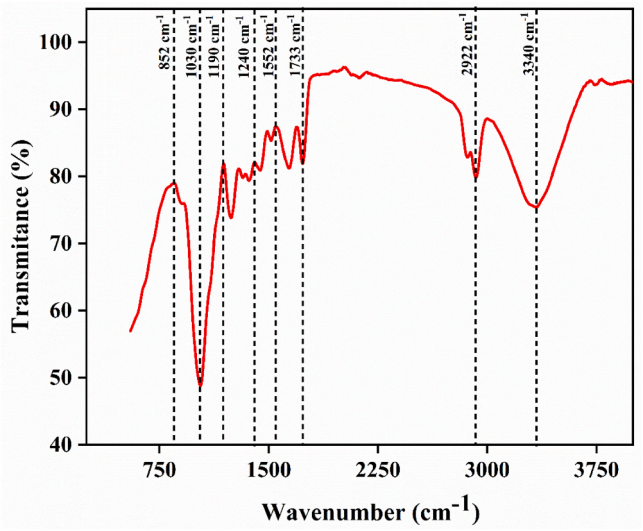

Fig. 4. FTIR curve of AHS particle.

particle the TS and TM elevate by 16.39% and 21.62%, respectively. This increase in the property determines a positive correlation with an addition of AHS particles. Subsequently, the inclusion of 10 wt% AHS particles provides a peak TS of 27.67 MPa and TM of 2.6 GPa, with an uplift of 24.14% and 15.55%, respectively compared to 5 wt% AHS particle loaded composites. *Polyalithia longifolia* seed filler reinforced composites exhibited a similar trend where the tensile strength rose with the filler addition and attained a maximum value of 32.50 MPa at 10 wt % loading [34]. This increase in TS and TM is attributed to the presence of cellulosic content in the particle which leads to effective stress transfer and the ability of the reinforcement to strengthen and stiffen the composite. Further, the TS and TM decreases while loading the composite with 15 and 20 wt% AHS particles. This is due to non-uniformity in the arrangement of the particles along with the formation of agglomerates and micro voids that accelerates the cavities and such defective nature subsequently reduces the composite's load bearing capacity [35,36]. Moreover, the excess particle content disrupts the continuity of the matrix and leads to improper wetting [37]. Thus, the optimal AHS particle quantity for the higher TS and TM is found to be 10 wt%, and at this loading the material tends to possess a strong filler-matrix interface, better particle dispersion and effective stress transfer.

As illustrated in Fig. 5(b) the flexural strength (FS) and flexural modulus (FM) of 5 wt% AHS particle loaded composite is evaluated to be 34.56 MPa and 2.2 GPa which is 18.96% and 30.97% higher than the FS and FM of NE, respectively. The further addition of particles

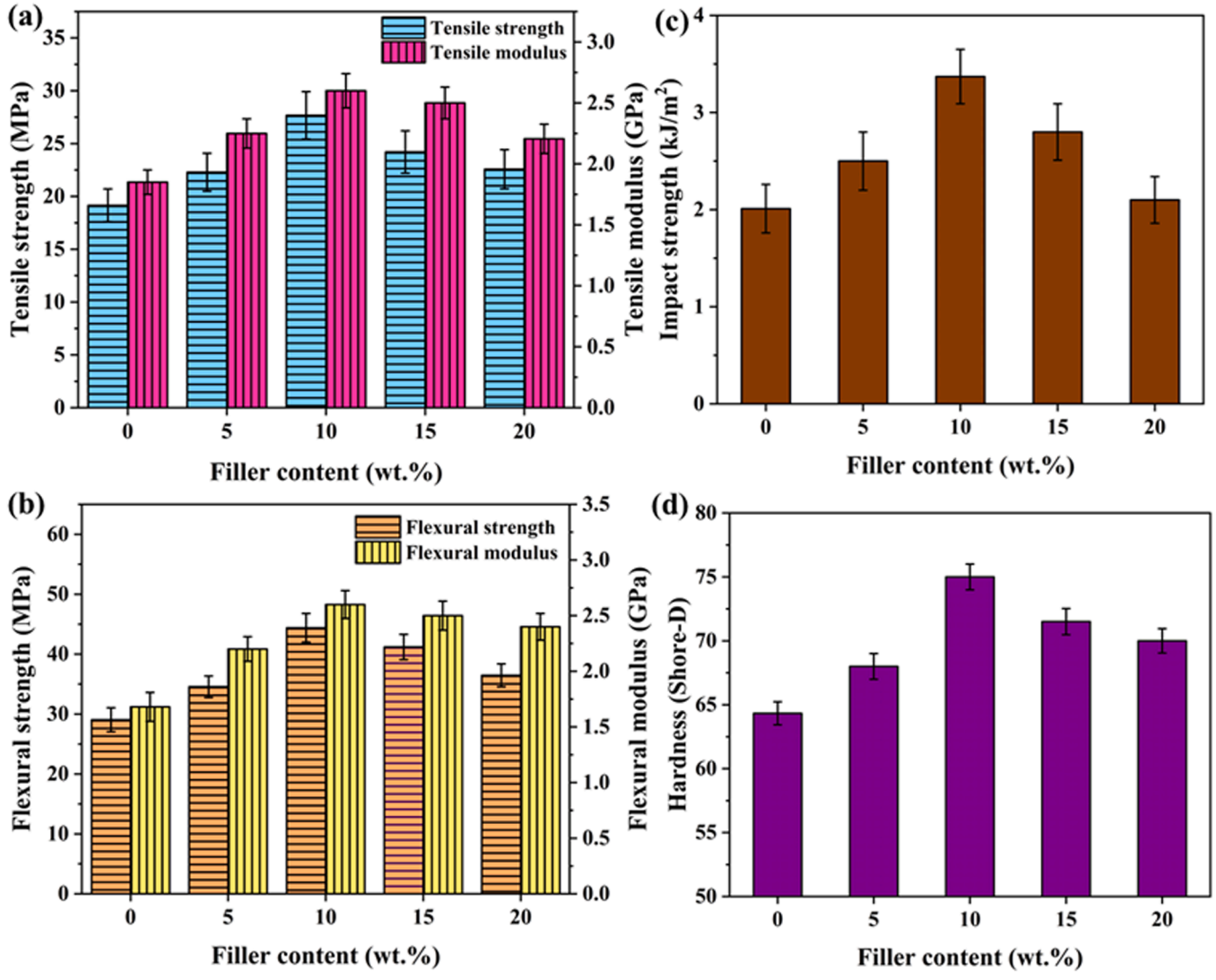

Fig. 5. Mechanical properties of AHS particle-based composites: (a) Tensile, (b) Flexural, (c) Impact, and (d) Hardness.

increased the bending strength of composites, especially the composites added with 10 wt% of AHS particles attains the maximum FS of 44.39 MPa and FM of 2.6 GPa. This is due to the rigidity and successive stress transfer within the material [38]. Similar pattern was seen in *Phoenix sp.* filler reinforced epoxy composites where flexural strength and modulus increased with filler addition and attained a maximum value of 53.31 MPa and 3.09 GPa respectively at 10 wt% loading [39]. Conversely, the FS and FM reduced when the material was loaded with 15 and 20 wt% AHS particles. The excess amount of particle accumulates as clusters and forms poor interface with the matrix [40]. Also, these agglomerates block the even spreading of particles in all directions in the matrix which reduced the flexural property of the composites.

The variation in impact strength (IS) of the samples due to changes in reinforcement quantity is shown in Fig. 5(c). It is observed that the IS of 5 wt% particle added composite is 24.38% more than the NE, which attribute to the ability of the AHS particles to prevent further propagation of cracks at certain regions [41]. Similarly, for the composite with 10 wt% particle content, the IS increases to a maximum of 3.37 kJ/m^2 which is the result of uniformity in particles spreading throughout the matrix [42]. On further increasing the concentration of particle to 15 and 20 wt%, the IS decreases as excess addition of particle creates stress at specific points which decreases the potential of the material to absorb impact energy caused due to sudden force. Furthermore, the increase in particle lowers the bonding between the particle and the matrix due to which failure occur at less impact load [41].

Fig. 5(d) signifies variation in hardness of composites reinforced with varied amount of AHS particles. The hardness of NE is noted to be 64.33, whereas the hardness of 5 wt% AHS particles reinforced composite is determined as 68 which confirms that the addition of seed particle creates a strong interphase with matrix that enhances the rigidity of the composite structure. The hardness of the 10 wt% filled composite is observed to be 75 and this could be attributed to the increased density and adhesion in the composites and resistance to the stretching of matrix molecules [43]. On further increase in the reinforcement content a gradual decline in hardness is noted and this decrease can be referred to the fact that increment in particles causes defects and stress concentrations at certain sites of the composite that invariably detriments the hardness value [44].

3.5. TGA and DTG

Thermal stability and degradation behavior of the AHS particles loaded composites were determined using TGA and its derivative (DTG). Fig. 6(a) illustrates the weight loss of the composite with increasing temperature up to 825 ℃ for various AHS particle contents. The TGA curve reveals a tripartite degradation pattern governed by the competitive breakdown of the lignocellulose constituents and the cross-linked epoxy. In the initial stage (dehydration phase), the degradation occurs in the temperature range of 29–266 ℃, exhibiting a relatively constant weight loss of 2 – 4% for all variations of composites. The minor weight loss corresponds to the evaporation of moisture (29–100 ℃), desorption of physically bound water from the hydroxyl group of AHS particles (100–200 ℃) as indicated in FTIR analysis, and removal of low-molecular-weight volatiles (200–266 ℃), such as residual solvent, natural fats, and waxes inherent to the seed. Notably, the onset of hemicellulose degradation falls in the initial stage due to its thermally unstable amorphous structure, which starts to degrade above 200 ℃ [45]. The primary pyrolytic degradation occurs in stage II, with a decomposition of hemicellulose, cellulose, and the epoxy matrix. This greater weight loss (80.1%) is primarily due to the simultaneous degradation of the cross-linked epoxy matrix and the cellulosic AHS particles. Observation revealed that the weight loss percentage was slightly higher for the NE and the 20 wt% AHS particle added composite compared to the 5, 10 and 15 wt% variations. In the case of NE, weight loss is attributed to the rapid depolymerization and absence of reinforcement to resist thermal degradation. Conversely, the weight loss for

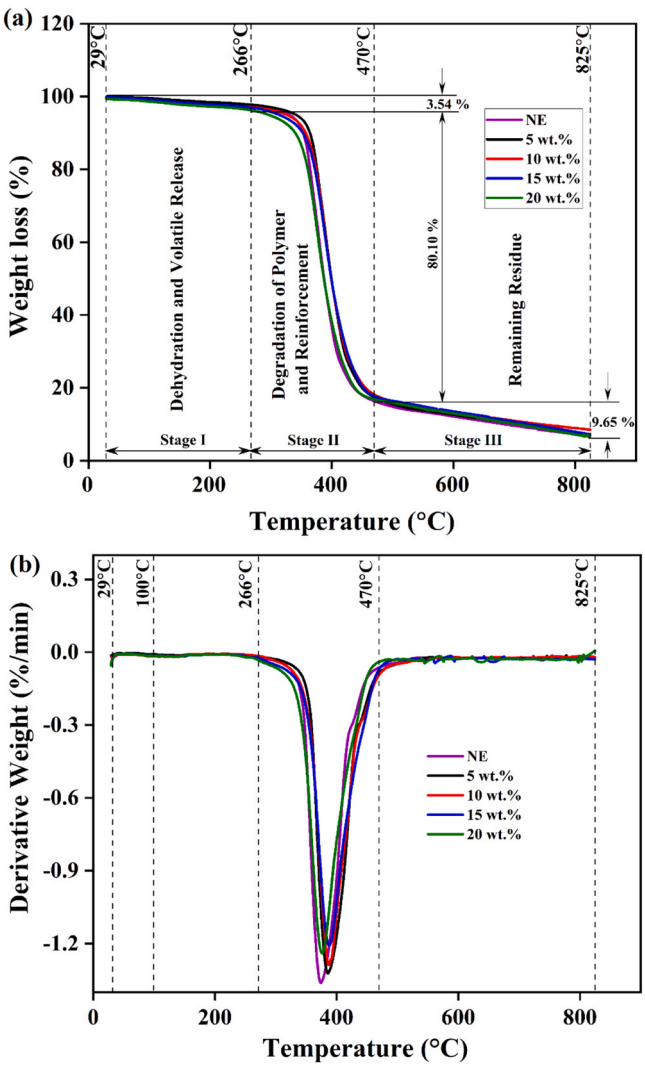

Fig. 6. Thermal analysis of AHS particle-based composites: (a) TGA curve, and (b) DTG curve.

the composite containing 20 wt% AHS particles may be due to the increased concentration of hemicellulose [46], and increased particle content leads to agglomeration and weaker interfacial bonding, which reduces the ability of the reinforcement as a thermal barrier and facilitates faster heat transfer within the composites. Intermediate loading (5–15 wt%) exhibits relatively lower weight loss due to the better dispersion of AHS particles and strong adhesion within the composites [47]. In the final stage, the residual mass of 10 wt% particle loaded composites are 1.27 times higher than NE and relatively higher than other composites. While it is theoretically expected that the 20 wt% added composites would yield a higher residue due to the increased mineral and lignin contents, but the results indicate a different trend [48]. This may be attributed to particle agglomeration, which causes localized heat concentration areas promoting greater thermal degradation [49]. Similar to this, the composites containing 10 – 15 wt% of *Phoenix sp.* fillers exhibited enhanced thermal stability attributable to improved epoxy-filler interactions [39].

DTG helps to identify the peak stability parameter for the TGA curve that characterizes the thermal decomposition kinetics of the AHS particle-based composites. Fig. 6(b) illustrates the DTG curve, which reveals a prominent peak between 266 – 470 ℃. This peak corresponds to the breakdown of cellulose and hemicellulose. Furthermore, it is evident from the Table 2, that the degradation temperature increases for composites added with AHS particles and shows a higher temperature

for the composites incorporated with 15 wt% of AHS particles. These increments imply that the incorporation of AHS particles increases the thermal stability of the epoxy matrix.

3.6. DSC

DSC helps to measure the energy absorbed or released by the sample, and its curve demonstrates the heat flow in the composites in terms of temperature. The results indicate that the NE demonstrate a heat-absorbing (endothermic) transition while AHS particles-reinforced epoxy matrix exhibit a heat-releasing (exothermic) transition (Fig. 7). The heat-absorbing peaks observed in the NE exhibits relatively a lower heat flow value of 19.55 mW, which is attributed to the polymer chain relaxation. On contrary, the 5 – 20 wt% AHS particles added composite exhibits heat flow values ranging from approximately 21–23 mW, along with noticeable exothermic transition in the temperature range of 65–75 ℃. This exothermic behavior can be related to the residual curing reaction and interaction between AHS particles and epoxy matrix, which may restrict the motion of polymer chain and alter the composite's thermal response [50]. The maximum heat flow of 22.75 mW was recorded for the composite with 5 wt% AHS particles, which is likely a result of stronger interfacial bonding and enhanced distribution of particles within the epoxy matrix, which eventually strengthens the material's structural and thermal integrity [51]. A similar trend of observation was reported by Rajeshkumar et al. [39], where the composite containing 5 wt% filler exhibited an exothermic peak intensity of 24.22 mW, indicating comparable thermal behavior at lower filler loadings. On further increasing the AHS particle content the energy releases per second declined. This reduction may be due to the insufficient wetting of particles and weakened interfacial interaction.

3.7. Water absorption

The amount of moisture absorbed by the AHS particle incorporated composites with respect to the immersion time is presented in Fig. 8(a). It is evidence that the increase in particle concentration increased the amount of water absorption which is the outcome of the hydrophilic nature of AHS particles. However, the water absorption reached saturation state around 70 hrs of soaking time. The water absorption in epoxy composites is modulated by voids content in composite, permeability of particle, immersion temperature, water-soaked area, quantity of particle and its dispersion [52]. The intrusion of moisture into the composite causes the water molecules to diffuse and adhere to the particle's hydrophilic groups, generating an intermolecular bond between the hydrogen and particle which improves the water intake ability [53]. However, the hydrophilic nature of the particles does not completely alter the hydrophobic nature of the composite (due to smaller particle size) rather, it persists with lesser the hydrophobic capacity [54].

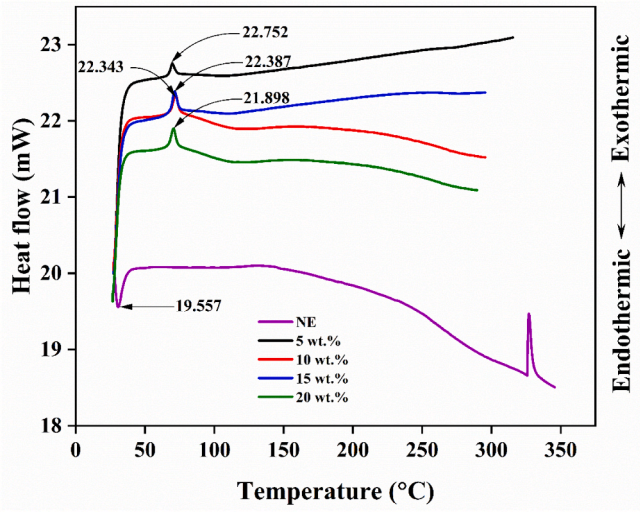

Fig. 7. DSC curves of AHS particle-based composites.

The water absorption tendency of AHS particle composites was further studied by understanding the water penetration mechanism and diffusion kinetics based on Fick's law, where the diffusion parameter 'n' is equal to 0.5 for Fickian diffusion [55]. For this, the experimental data were fitted to the Eq. (4) [56], and the fitted curve is shown in Fig. 8(b).

$$\log\left(\frac{M_t}{M_{sat}}\right) = \log(k) + n\log(t) \tag{4}$$

where, M_t and M_{sat} are the quantity of water intake at time 't' and at saturation point, respectively; k and n are the constants. The value of n is found to be in the spectrum of 0.43–0.58 (Table 3), which confirms the behavior of Fickian diffusion. Moreover, the coefficient of determination (R^2) value for all formulations approached unity, indicating an excellent agreement between predicted model and experimental data. The rate of moisture transport into the composites is given by diffusion coefficient (D), whose value is determined by the Eq. (5) [55].

$$D = \pi\left[\frac{h}{4M_{sat}}\right]^2\left[\frac{M_b - M_a}{\sqrt{T_b} - \sqrt{T_a}}\right]^2 \tag{5}$$

where, h is specimen thickness (mm), T_a and T_b are time period between the linear region of the absorption curve, M_a and M_b are percentage of water absorption at time T_a and T_b. Furthermore, two important parameters, absorption coefficient (S) and Permeability (P) are determined to completely understand the sorption kinetics. The absorption coefficient (S) is calculated to find the extent of penetrant uptake using the Eq. (6) [55].

$$S = \frac{M_{sat}}{M_c} \tag{6}$$

And permeability is given by,

$$P = D \times S \tag{7}$$

where, m_c denotes the mass of the composite sample. The findings revealed that, with increase in filler quantity the values of D, P and S also increase, indicating the hydrophilic nature of the filler, which facilitates faster and easier penetration of water.

Furthermore, the water contact angle measurement shown in the Fig. 8(c), also demonstrates the hydrophilic nature of composites. It is important to note that, at lower filler loadings, the filler particles were evenly distributed in the matrix, with better interfacial adhesion and reasonably compact surface structure. This decreased the hydrophilic sites at the surface of the composite and hence increased the contact angle. However, the contact angle was reduced with increase filler content due to agglomeration of the particles, weak interfacial bonding and creation of micro voids. These flaws enhance water uptake and expose more hydrophilic hydroxyl groups from the lignocellulosic filler, thus enhancing the surface wettability [16].

3.8. Failure mechanism

The SEM image of fractured surface of AHS particle added composites is shown in Fig. 9. The formation of craters observed in Fig. 9(a) is due to hydrophilic nature of the filler and hydrophobic nature of epoxy which leads to incompatibility between the filler and the matrix, moreover there is a shrinkage effect during curing period of the composite which leads to debonding of the reinforcements [57]. The number of craters will be more in the case of composites loaded with higher filler contents which may acts as a stress concentration zone leads to reduced mechanical properties. Fig. 9(b) depicts the matrix crack which arises

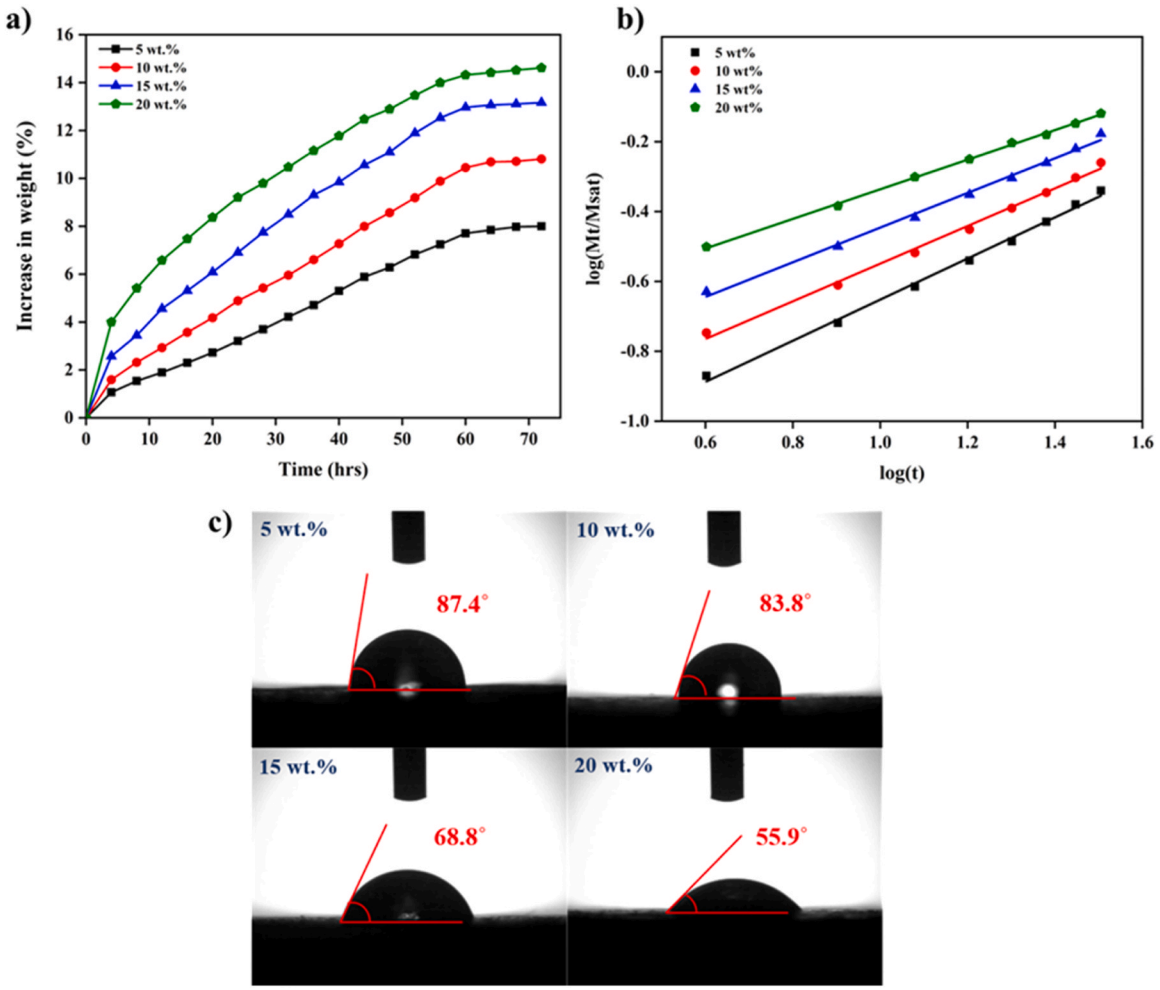

Fig. 8. Water uptake pattern: (a) water absorption, (b) water kinetics, (c) water contact angle.

Table 3
Water kinetic parameters of AHS particle loaded composites.

AHS content (wt%)	Saturated water absorption M_{sat} (%)	Diffusion coefficient 10^{-10} (D) (m^2 /min)	Absorption coefficient (S) (g/g)	Permeability coefficient 10^{-11} (P) (m^2/min)	n	k
5	7.607	1.66	0.0662	1.1	0.43	0.1741
10	10.81	2.11	0.981	2.07	0.58	0.0575
15	13.06	3.49	0.1209	4.22	0.53	0.0818
20	14.32	5.25	0.1331	6.99	0.50	0.1144

from stress concentration sites due to mechanical loading, and their propagation is limited due to the existence of AHS particle having good interfacial bonding with matrix. Fig. 9(c) exhibits uniform dispersion of particle which ensures effective stress transfer and boost the load bearing capacity of the material [6]. These are responsible for enhanced mechanical performance of the composites. Moreover, increase in the amount of particle enables agglomeration within the matrix at certain sites which are prone to destruction due to the insufficient bonding which affects the ability to support loads and influences the stress transfer within the composites Fig. 9(d) [58].

4. Conclusions

In this study, the composites were fabricated by varying the content of AHS particles and investigated their physical, mechanical, morphological, and thermal properties. The presence of cellulose in AHS particles is noted in FTIR analysis and XRD analysis infers the crystalline size (14.03 nm) and index (10.8%) of AHS particles. The tested composite sample attained a peak tensile, flexural and impact strengths of 27.67 MPa, 44.39 MPa, and 3.37 kJ/m^2, respectively at 10 wt percentage filler loading, indicating that the addition of AHS particles improved the mechanical properties of the epoxy. Accordance with Fickian diffusion mechanism the higher AHS particle content allows the water with faster penetration and the contact angle impose the hydrophilic nature of AHS particles. SEM analysis revealed the presence of craters, voids, micro-cracks and particle agglomeration at higher filler loadings is identified as the primary failure mechanism. The results of TGA showed that the composite with 15 wt% AHS particles possessed the highest thermal stability at 387.45 °C. Furthermore, the onset of major degradation occurred later in the composites (compared to NE), indicating improved thermal resistance. The DSC results indicate the presence of an endothermic peak in NE, whereas the AHS particles-reinforced epoxy matrix exhibit an exothermic transition. The latter results from the augmented crosslinking reactions prompted by the AHS

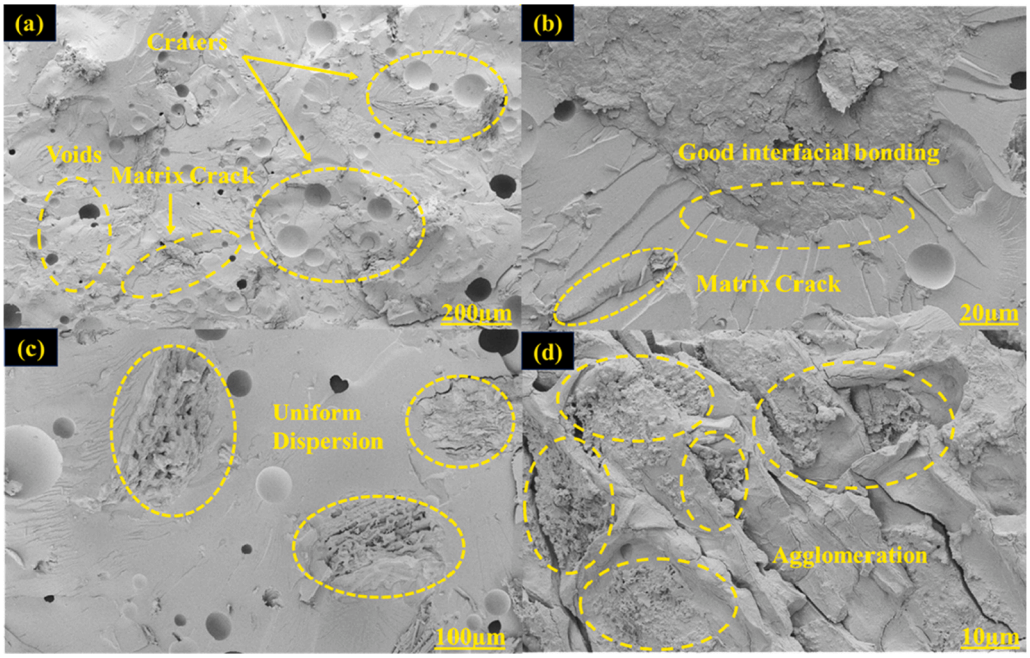

Fig. 9. Fractographic images of mechanical tested AHS particle composites.

particles, signifying enhanced temperature stability and interfacial interactions. Overall, including AHS particles into the epoxy resulted in light weight composites at a reasonable cost, as well as significant mechanical and thermal qualities that aligned with sustainable development goals (SDG 9 and 12). The developed composites have low density, adequate mechanical performance and enhanced thermal stability, which demonstrates their potential for application in lightweight structural and semi-structural applications such as automotive interior components, ceiling panels, wall panels, partition boards and household and sporting products.

CRediT authorship contribution statement

S.V. Naren Prasaadh: Writing – original draft, Validation, Methodology, Investigation. **G. Rajeshkumar:** Writing – original draft, Supervision, Methodology, Investigation, Conceptualization. **S. Prithika:** Writing – review & editing, Visualization, Validation, Formal analysis, Data curation. **S. Keerthika:** Writing – original draft, Software, Resources, Project administration, Methodology. **T. Rohith Sai:** Writing – review & editing, Validation, Supervision, Conceptualization.

Declaration of Competing Interest

The authors declare that they have no known competing financial interests or personal relationships that could have appeared to influence the work reported in this paper.

References

[1] J.K. Singh, Experimental investigation on physical, mechanical, thermal, and morphological behaviour of silane-modified Borassus flabellifer leaflet fibre reinforced polymer nanocomposites (no. July), Materials 9 (2025) 0–2, https://doi.org/10.1016/j.nxmate.2025.100989.
[2] I. Bianchi, A. Forcellese, I. Taha, Comparative LCA of fully biobased and synthetic polymer composites accounting for fiber treatment (no. October), J. Clean. Prod. 530 (2025) 146846, https://doi.org/10.1016/j.jclepro.2025.146846.
[3] S. Palanisamy, T.M. Murugesan, M. Palaniappan, C. Santulli, N. Ayrilmis, Use of hemp waste for the development of mycelium-grown matrix biocomposites: a concise bibliographic review, BioResources 18 (4) (Nov. 2023) 8771–8780, https://doi.org/10.15376/biores.18.4.Palanisamy.
[4] N.S. Ra, et al., Isolation and characterization of agro-waste biomass sapodilla seeds as reinforcement in potential polymer composite applications, Heliyon 9 (7) (2023) e17760, https://doi.org/10.1016/j.heliyon.2023.e17760.
[5] V. Johny, A. Kuriakose Mani, S. Palanisamy, V.K. Rajan, M. Palaniappan, C. Santulli, Extraction and PHysico-chemical Characterization of Pineapple Crown Leaf Fibers (PCLF), Fibers 11 (1) (Jan. 2023) 5, https://doi.org/10.3390/fib11010005.
[6] A. Saha, S. Kumar, A. Kumar, Influence of pineapple leaf particulate on mechanical, thermal and biodegradation characteristics of pineapple leaf fiber reinforced polymer composite, J. Polym. Res. 28 (2) (2021) 66, https://doi.org/10.1007/s10965-021-02435-y.
[7] Budi Susetyo, H.P.S.A. Khalil, M.S. Rahul Dev Bairwan, Rimun Wibowo, and N.F. M. Rawi, Harnessing agro-food organic residues for biodegradable materials: Toward circular and sustainable solutions, *Bioresour. Technol. Reports*, doi: https://doi.org/10.1016/j.biteb.2025.102396.
[8] I. Suyambulingam, R. Kumar, S.S. Saravanakumar, T.S. Senthilkumar, Natural particulate reinforced biocomposite film: a review, J. Nat. Fibers 22 (1) (2025), https://doi.org/10.1080/15440478.2025.2500641.
[9] 1 Muhammad Mujtaba a, b et al., Lignocellulosic biomass from agricultural waste to the circular economy: a review with focus on biofuels, biocomposites and bioplastics, *J. Clean. Prod.*, doi: https://doi.org/10.1016/j.jclepro.2023.136815.
[10] M.S. Fadly, Kusmono, M.W. Wildan, K. Wahyudi, R.A. Ilyas, Comparative study of physical, mechanical, thermal, and morphological properties of raw, alkali, and 3-aminopropyltriethoxysilane (APTES)-treated Agave angustifolia Haw fibers for green-composite reinforcement, Mater 11 (March) (2026) 101948, https://doi.org/10.1016/j.nxmate.2026.101948.
[11] K.P. Srinivasa Perumal, L. Selvarajan, K.P. Manikandan, C. Velmurugan, Mechanical, tribological, and surface morphological studies on the effects of hybrid ilmenite and silicon dioxide fillers on glass fibre reinforced epoxy composites, J. Mech. Behav. Biomed. Mater. 146 (2023) 106095, https://doi.org/10.1016/j.jmbbm.2023.106095.
[12] C. Balaji Ayyanar, et al., Sustainable LDPE composites reinforced with Syzygium cumini seed biofillers: mechanical, thermal, and morphological performance assessment, Materials 11 (March) (2026) 101795, https://doi.org/10.1016/j.nxmate.2026.101795.
[13] M. Dawoua Kaoutoing, et al., Characterisation of a composite material with polyester matrix reinforced with particles from doum palm (Hyphaene thebaica) fruit, Results Mater. 18 (September 2022) (2023), https://doi.org/10.1016/j.rinma.2023.100401.
[14] M.P. Vengatesh, B. Stalin, V. Vignesh, N. Nagaprasad, Development and analysis of T. Arjuna Seed/Vinyl-Ester composite materials for lightweight automotive components, Polym. Bull. 83 (4) (2026), https://doi.org/10.1007/s00289-025-06245-w.
[15] K. Murugananthan, S. Senthil, P. Senthamaraikannan, R. Kumar, Use of caesalpinia bonducella seed shell waste as filler for reinforcement in epoxy composites use of caesalpinia bonducella seed shell waste as filler for, J. Nat. Fibers 22 (1) (2025), https://doi.org/10.1080/15440478.2025.2475159.
[16] G. Rajeshkumar, A. Poovarasan, S.V.N. Prasaadh, M.R. Sanjay, S. Siengchin, Effectiveness of Phoenix sp. particles as reinforcement in epoxy composites: mechanical, free vibration, thermal, and water absorption characteristics, Results Eng. 29 (July 2025) (2026) 109291, https://doi.org/10.1016/j.rineng.2026.109291.

[17] J. Zhu, C. Abeykoon, N. Karim, Investigation into the effects of fi llers in polymer processing, Int. J. Light. Mater. Manuf. 4 (3) (2021) 370–382, https://doi.org/10.1016/j.ijlmm.2021.04.003.
[18] J.C. Capricho, B. Fox, N. Hameed, Multifunctionality in epoxy resins, Polym. Rev. 60 (1) (2020) 1–41, https://doi.org/10.1080/15583724.2019.1650063.
[19] X. Mi *et al.*, Toughness and its mechanisms in epoxy resins, 2022. doi: 10.1016/j.pmatsci.2022.100977.
[20] K.P. Rajesh and L. Sharma, Herbal Remedies: A Revitalizing Strategy for Treating Human Illnesses, Including Key Ingredients, Preparations, Current Situation, and Prospects for the Future, vol. 9, no. 12, pp. 1–14, 2025.
[21] A.V. PURI, Artabotrys hexapetalus (L.F) Bhandari: a plant with biomedical potential, Int. J. Pharm. Pharm. Sci. 12 (6) (2020) 8–14, https://doi.org/10.22159/ijpps.2020v12i6.37778.
[22] T. Handayani, Seed germination and seedling morphology of Artabotrys hexapetalus, Nusant. Biosci. 9 (1) (2017) 23–30, https://doi.org/10.13057/nusbiosci/n090105.
[23] S. Zhang, X. Wang, J. Yang, H. Chen, X. Jiang, Micromechanical interlocking structure at the filler/resin interface for dental composites: a review, Int. J. Oral. Sci. 15 (1) (2023), https://doi.org/10.1038/s41368-023-00226-3.
[24] K.P. Srinivasa Perumal, L. Selvarajan, P. Mathan Kumar, S. Shriguppikar, Enhancing mechanical and morphological properties of glass fiber reinforced epoxy polymer composites through rutile nanoparticle incorporation, Prog. Addit. Manuf. 10 (1) (2025) 831–848, https://doi.org/10.1007/s40964-024-00675-0.
[25] H.J. Rao, S. Singh, H. Pulikkalparambil, P.J. Ramulu, S.M. Rangappa, S. Siengchin, Extraction of cellulosic filler from artocarpus heterophyllus (jackfruit) as a reinforcement material for polymer composites, J. Polym. Environ. 31 (2) (2023) 479–487, https://doi.org/10.1007/s10924-022-02651-7.
[26] K. Murugananthan, S. Senthil, P. Senthamaraikannan, R. Kumar, Use of caesalpinia bonducella seed shell waste as filler for reinforcement in epoxy composites, J. Nat. Fibers 22 (1) (2025), https://doi.org/10.1080/15440478.2025.2475159.
[27] M. Palaniappan, et al., Influence of washing with sodium lauryl sulphate (SLS) surfactant on different properties of ramie fibres, BioResources 19 (2) (Mar. 2024) 2609–2625, https://doi.org/10.15376/biores.19.2.2609-2625.
[28] N. Terinte, R. Ibbett, and K.C. Schuster, Overview on native cellulose and microcrystalline cellulose I structure studied by X-ray diffraction (WAXD): Comparison between measurement techniques Oveview on native cellulose and microcrystalline cellulose I structure studied by X- Ray diffraction (vol. 89, no. January 2011, pp. 118–131, 2017.
[29] S. Hossain, M.A. Jalil, T. Islam, M.M. Rahman, A low-density cellulose rich new natural fiber extracted from the bark of jack tree branches and its characterizations, Heliyon 8 (11) (2022), https://doi.org/10.1016/j.heliyon.2022.e11667.
[30] A. Hejna, M. Sulyman, M. Przybysz, M.R. Saeb, M. Klein, K. Formela, On the correlation of lignocellulosic filler composition with the performance properties of poly(ε-caprolactone) based biocomposites, Waste Biomass-.-. Valoriz. 11 (4) (2020) 1467–1479, https://doi.org/10.1007/s12649-018-0485-5.
[31] T. Khuntia, S. Biswas, Characterization of a novel natural filler from sirisha bark, J. Nat. Fibers 19 (8) (2022) 3083–3092, https://doi.org/10.1080/15440478.2020.1838997.
[32] D. Dhanabalan, et al., Experimental investigation of date seed and neem powder reinforced natural fiber composites, Medziagotyra 30 (3) (2024) 334–339, https://doi.org/10.5755/j02.ms.34033.
[33] D.T. Arunkumar, et al., Fabrication and characterization of acacia leucophloea bark fiber-reinforced epoxy composites with lotus seed shell powder as a sustainable bio-filler, Results Eng. 29 (2025) (2026) 108342, https://doi.org/10.1016/j.rineng.2025.108342.
[34] B. Stalin, et al., Evaluation of mechanical, thermal and water absorption behaviors of Polyalthia longifolia seed reinforced vinyl ester composites, Carbohydr. Polym. 248 (2020) 116748, https://doi.org/10.1016/j.carbpol.2020.116748.
[35] J.O. Agunsoye, S.A. Bello, L.O. Adetola, Experimental investigation and theoretical prediction of tensile properties of Delonix regia seed particle reinforced polymeric composites, J. King Saud. Univ. - Eng. Sci. 31 (1) (2019) 70–77, https://doi.org/10.1016/j.jksues.2017.01.005.
[36] S. Siraj, A.H. Al-Marzouqi, M.Z. Iqbal, W. Ahmed, Impact of micro silica filler particle size on mechanical properties of polymeric based composite material, Polymers 14 (22) (2022), https://doi.org/10.3390/polym14224830.
[37] I.O. Oladele, A.S. Taiwo, L.J. Bello, S.O. Balogun, L. Senzeni Sipho, S.O. Adelani, Fabrication of animal shell and sugarcane bagasse particulate hybrid reinforced epoxy composites for structural applications, Polym. Polym. Compos. 32 (2024) 1–12, https://doi.org/10.1177/09673911231202183.
[38] H.T.N. Kuan, M.Y. Tan, Y. Shen, M.Y. Yahya, Mechanical properties of particulate organic natural filler-reinforced polymer composite: A review, 263498332110075, Compos. Adv. Mater. 30 (2021), https://doi.org/10.1177/26349833211007502.
[39] G. Rajeshkumar, A. Poovarasan, S.V.N. Prasaadh, M.R. Sanjay, S. Siengchin, Effectiveness of Phoenix sp. particles as reinforcement in epoxy composites: mechanical, free vibration, thermal, and water absorption characteristics, Results Eng. 29 (2026) 109291, https://doi.org/10.1016/j.rineng.2026.109291.
[40] I. Khan, N. Kumar, M. Choudhary, S. Kumar, T. Singh, Mechanical and dynamic mechanical behavior of 3D printed waste slate particles filled acrylonitrile butadiene styrene composites, Arab. J. Chem. 17 (2) (2024) 105559, https://doi.org/10.1016/j.arabjc.2023.105559.
[41] R.O. Akaluzia, F.O. Edoziuno, A.A. Adediran, B.U. Odoni, S. Edibo, T.M. A. Olayanju, Evaluation of the effect of reinforcement particle sizes on the impact and hardness properties of hardwood charcoal particulate-polyester resin composites, Mater. Today Proc. 38 (xxxx) (2021) 570–577, https://doi.org/10.1016/j.matpr.2020.02.980.
[42] R.V. Saikumar Reddy, L.R. Jeeru, P. Venkateshwar Reddy, K. Swamy, Mechanical properties evaluation of pomegranate peel powder filled jute fiber reinforced epoxy composites, Mater. Today Proc. 62 (2022) 6923–6926, https://doi.org/10.1016/j.matpr.2021.12.043.
[43] I.O. Oladele, et al., Eggshell bio-derived hydroxyapatite particle-wool/polyester staple fibers hybrid reinforced epoxy bio-composites for biomedical services, Hybrid. Adv. 7 (2024) 100312, https://doi.org/10.1016/j.hybadv.2024.100312.
[44] G. Vyshnava Kumar, G.B. Rao, S.J.J. Marshal, P.K. Bannaravuri, S.S. Joel, G. J. Calvin, Effect of bamboo leaf and pista shell powder particles on mechanical and wear behaviour of polymer composites, J. Inst. Eng. Ser. D. 105 (2) (2024) 911–921, https://doi.org/10.1007/s40033-023-00558-8.
[45] N.M. Nurazzi, et al., Thermogravimetric analysis properties of cellulosic natural fiber polymer composites: a review on influence of chemical treatments, Polymers 13 (16) (2021), https://doi.org/10.3390/polym13162710.
[46] J.S.S. Neto, H.F.M. de Queiroz, R.A.A. Aguiar, M.D. Banea, A review on the thermal characterisation of natural and hybrid fiber composites, Polymers 13 (24) (2021), https://doi.org/10.3390/polym13244425.
[47] H.I. Umaru, U.S. Ishiaku, M.K. Yakubu, A.A. Kogo, N. Lawal, Effect of particle size on the mechanical, water absorption and thermal properties of flamboyant seed particle-filled polyester composites for tile applications, Caliphate J. Sci. Technol. 7 (1) (2025) 34–43, https://doi.org/10.4314/cajost.v7i1.5.
[48] S. Kolawole, et al., Thermogravimetry analysis of epoxy and unsaturated polyester filled with some agricultural waste of dates palm (phoenix dactylifera) and african elemi (canarium shweinfurthii) particulate composites, J. Mater. Sci. Res. Rev. 2 (3) (2019) 394–402.
[49] J.L. Thomason, J.L. Rudeiros-Fernández, Thermal degradation behaviour of natural fibres at thermoplastic composite processing temperatures, Polym. Degrad. Stab. 188 (2021), https://doi.org/10.1016/j.polymdegradstab.2021.109594.
[50] J.C. Lopez-Mercado, D. Mahecha-Rivas, J.P. Correa-Aguirre, J.P. Casas-Rodriguez, M.A. Hidalgo-Salazar, Development of natural fiber-epoxy and vinyl ester biocomposites for sustainable fabrication of hydrokinetic turbines, Materials 11 (December) (2026), https://doi.org/10.1016/j.nxmate.2026.101651.
[51] M. Mohammadi, M.R. Ishak, M.T. Hameed, Exploring chemical and physical advancements in surface modification techniques of natural fiber reinforced composite: a comprehensive review exploring chemical and physical advancements in surface modification techniques of natural fiber reinforced comp, J. Nat. Fibers 21 (1) (2024), https://doi.org/10.1080/15440478.2024.2408633.
[52] L.N. Onuh, et al., Optimizing biomedical facilities performance with dombeya fiber-paper particle hybrid reinforced epoxy composites, Sci. Eng. Technol. 4 (1) (2024) 14–31, https://doi.org/10.54327/set2024/v4.i1.114.
[53] A.Y. Al-Maharma, N. Al-Huniti, Critical review of the parameters affecting the effectiveness of moisture absorption treatments used for natural composites, J. Compos. Sci. 3 (1) (2019), https://doi.org/10.3390/jcs3010027.
[54] D. Jayabalakrishnan, P. Prabhu, S.M. Iqbal, V. Mugendiran, S. Ravi, V.R. Arun Prakash, Mechanical, dielectric, and hydrophobicity behavior of coconut shell biochar toughened Caryota urens natural fiber reinforced epoxy composite, Polym. Compos. 43 (1) (2022) 493–502, https://doi.org/10.1002/pc.26393.
[55] P. Sahu, M. Gupta, Water absorption behavior of cellulosic fibres polymer composites: a review on its effects and remedies, J. Ind. Text. 51 (5_) (Jun. 2022), https://doi.org/10.1177/1528083720974424.
[56] N.H.I. Kamaludin, H. Ismail, A. Rusli, S.S. Ting, Thermal behavior and water absorption kinetics of polylactic acid/chitosan biocomposites, Iran. Polym. J. (Engl. Ed. 30 (2) (2021) 135–147, https://doi.org/10.1007/s13726-020-00879-5.
[57] C.B. Ayyanar, K. Marimuthu, I.J. Das, C. Prakash, Investigation of coconut shell fillers loaded and pine apple fiber reinforced epoxy sandwich composites, J. Polym. Res. 31 (12) (2024) 353, https://doi.org/10.1007/s10965-024-04205-y.
[58] M.M.A. Nassar, B.J. Abu Tarboush, K.I. Alzebdeh, N. Al-Hinai, T. Pervez, New synthesis routes toward improvement of natural filler/synthetic polymer interfacial crosslinking, Polymers 14 (3) (2022), https://doi.org/10.3390/polym14030629.